SLAC–PUB–13545
February 2009

Generation of attosecond x-ray pulses with a multi-cycle two-color ESASE scheme*

Y. Ding[1], Z. Huang[1], D. Ratner[1], P. Bucksbaum[1], H. Merdji[2,1],

[1] SLAC National Accelerator Laboratory, Menlo Park, CA 94025, USA
[2] CEA/SPAM, Centre de Saclay, 91191 Gif sur Yvette, France

Abstract

Generation of attosecond x-ray pulses is attracting much attention within the x-ray free-electron laser (FEL) user community. Several schemes using extremely short laser pulses to manipulate the electron bunches have been proposed. In this paper, we extend the attosecond two-color ESASE scheme proposed by Zholents *et al.* to the long optical cycle regime using a second detuned laser and a tapered undulator. Both lasers can be about ten-optical-cycles long, with the second laser frequency detuned from the first to optimize the contrast between the central and side current spikes. A tapered undulator mitigates the degradation effect of the longitudinal space charge (LSC) force in the undulator and suppresses the FEL gain of all side current peaks. Simulations using the LCLS parameters show a single attosecond x-ray spike of ~ 110 attoseconds can be produced. The second laser can also be detuned to coherently control the number of the side x-ray spikes and the length of the radiation pulse.

Submitted to the Phys. Rev. ST Accel. Beams.

*Work supported in part by Department of Energy contract DE–AC02–76SF00515.

I. INTRODUCTION

Ultrashort soft and hard x-ray sources have the potential to open new regimes in atomic and electronic processes, benefiting widespread fields in physics, chemistry and biology. This has motivated the development of laser based ultrashort soft x-ray sources as well as the construction of fourth generation free electron laser (FEL) sources in the soft and hard x-ray regime. Due to the duration of the electron bunch, FEL facilities have aimed for the femtosecond regime, but the formidable challenge of generating attosecond pulses is attracting much attention within the x-ray FEL user community. Several schemes for generation of attosecond x-ray pulses have been proposed [1–8], mostly by manipulating of electron bunches with extremely short laser pulses.

The two-color scheme proposed in Ref. [6] is based on the current-enhanced self-amplified spontaneous emission (ESASE) technique proposed by Zholents [9]. The electrons interact with two short laser pulses within two single-period wiggler magnets to generate a time-dependent energy modulation in the bunch. A dispersive section, such as a four-dipole chicane, converts the energy modulation of the electron bunch to a density modulation. The high current spike formed by the overlapping peak intensities of the two lasers dominates the FEL gain process and produces an attosecond x-ray pulse. Ultra-short lasers with no more than two optical cycles are required to minimize satellite spikes. In addition, the longitudinal space charge (LSC) field in the main FEL undulator has to be considered properly [10].

In this paper, we extend the attosecond two-color ESASE scheme to the long optical cycle regime using a detuned second laser and a tapered undulator by taking advantage of the LSC field. Our scheme extends to FELs a technique proposed for high-order harmonic generation (HHG) to manipulate an electron wave packet for the generation of isolated attosecond soft X-ray pulses [11]. HHG experiments have shown a controlled detuning between the two colors can control the electron wave packet energy (low energy regime) in the sub-cycle domain using relatively long infrared laser pulses (up to 15 optical cycles). Here, we apply this idea to ESASE. Both lasers can be about ten optical cycles long, with the second laser frequency detuned from the first one to optimize the contrast between the central and side current spikes. A tapered undulator mitigates the degradation effect of the LSC force in the undulator [10] and suppresses the FEL gain of all side current spikes.

II. OPTIMIZATION OF THE ENERGY MODULATION

Our study is carried out for the Linac Coherent Light Source (LCLS) [13], but can be applied to other similar x-ray FEL facilities as well [14, 15]. We use similar electron beam parameters and accelerator setup as in Ref. [6], but with relatively long laser pulses of about 10 optical cycles or more. A schematic setup is shown in Fig. 1. The laser system, driven by a chirped-pulse amplification Ti:sapphire laser, produces carrier-envelope phase-stabilized pulses with a tunable central wavelength around 1.5 μm. This laser scheme was demonstrated in ref. [12]. The two-color laser and two one-period wigglers produce an energy modulation on the same portion of electrons. Then a 4-dipole chicane converts the electron beam energy modulation to density modulation. By optimizing the frequency of the second laser, the side peaks adjacent to the central peak of the electron bunch are expected to be small. Table I summarizes the main parameters for the electron beam, lasers and wigglers used in this study.

The energy modulation of the electrons after interaction with a laser can be calculated from the FEL equations, as described in Ref. [6]. Here we choose the fundamental laser (Laser-1) with a wavelength of 0.8 μm and a pulse duration of 25 fs (intensity FWHM), which is commercially available. Laser-1 is focused at the center of the first wiggler (W1), with its carrier wave phase adjusted to zero-crossing at the peak of the laser envelope. After interaction in the first wiggler (W1) with a laser power of 20 GW, the electrons have an energy modulation amplitude of 3.8 MeV at the center of the bunch. If we pass this beam through the chicane to optimize the density modulation for the central period, the side periods also form density peaks. We use a relatively long laser pulse here, so the side peaks in the current profile are not sufficiently suppressed by the envelope of the waveform. The current profile with Laser-1 modulation after the chicane is shown in Fig. 3 with red dotted curve.

We further optimize the energy modulation by tuning the second laser (Laser-2) frequency, intensity and pulse length. The wavelength of Laser-2 is optimized to be at 1.314 μm with a pulse duration of 45 fs (intensity FWHM). To make an effective energy modulation, Laser-2 interacts at the center of the second wiggler (W2) with the same portion of the electron bunch, also at zero-crossing phase. After interacting in W2, the electrons at the bunch center gain an additional energy modulation of 1.7 MeV, while electrons at

the neighboring periods lose some energy modulation due to the frequency detuning. Fig. 2 shows the combined energy modulation of the electrons after interacting with the two lasers. The total energy modulation amplitude at the center of the bunch is 5.5 MeV. The bunching chicane is set at $R_{56} = 380\mu$m to fully compress the central period of the energy-modulated bunch. The resulting current profile after the dispersive section is shown in Fig. 3 with solid blue curve. We obtain a contrast ratio between the central peak and the side maximum peak of 17kA/11kA, which is much better than for the single laser case (red dotted curve in Fig. 3).

TABLE I: Main parameters for electrons, lasers and wigglers

	parameter	**value**	**unit**
Electron	energy	13.6	GeV
	peak current	3.4	kA
	rms emittance	1.2	μm
	rms energy spread	1.1	MeV
Laser-1	wavelength	0.8	μm
	power	20	GW
	FWHM of intensity	25	fs
Laser-2	wavelength	1.314	μm
	power	2.4	GW
	FWHM of intensity	45	fs
Wiggler-1	period	0.5	m
	wiggler parameter K_{w1}	67.3	
Wiggler-2	period	0.5	m
	wiggler parameter K_{w2}	86.3	
Chicane	R_{56}	380	μm
FEL	Undulator period	3	cm
	undulator parameter K	3.5	
	average beta function	18	m
	wavelength	1.5	Å

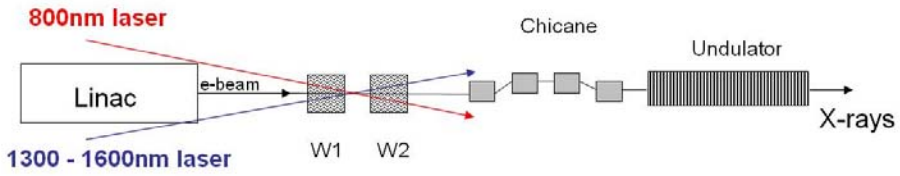

FIG. 1: (color) Schematic setup for the two-color ESASE.

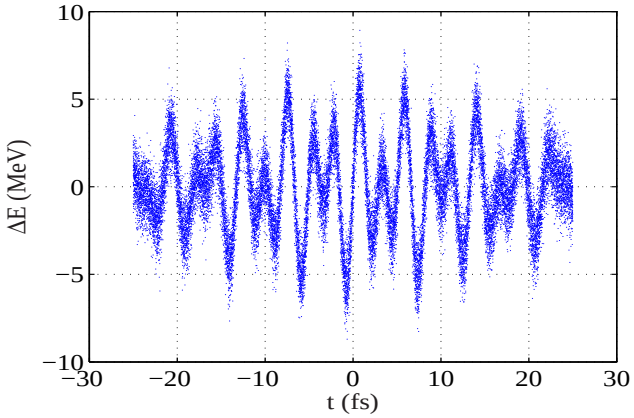

FIG. 2: (color) Calculated longitudinal phase space of the electrons after interaction with two lasers.

III. LONGITUDINAL SPACE CHARGE IN THE FEL UNDULATOR

After the bunching chicane, the energy modulation is converted to a density modulation, giving a peak current of 17 kA in the central spike for our case, as shown in Fig. 3. Since only a small section of the bunch charge is concentrated in the spike region, the emittance growth due to coherent synchrotron radiation in the chicane and transverse space charge in the main undulator is negligible. However, due to the wiggling motion in the undulator, the longitudinal space charge field is equivalent to the free space result by changing γ to $\bar{\gamma}_z$, where $\bar{\gamma}_z = \gamma/\sqrt{1+K^2/2}$, and K is the undulator parameter [10]. In the limit when the electron bunch length in the average comoving frame is much larger than the transverse beam size, we can use a simplified expression to estimate the longitudinal space charge field [16]:

$$E_z \approx -\frac{Z_0 I'(s)}{4\pi\bar{\gamma}_z^2}\left(2\ln\frac{\bar{\gamma}_z\sigma_z}{r_b} + 1 - \frac{r^2}{{r_b}^2}\right), \tag{1}$$

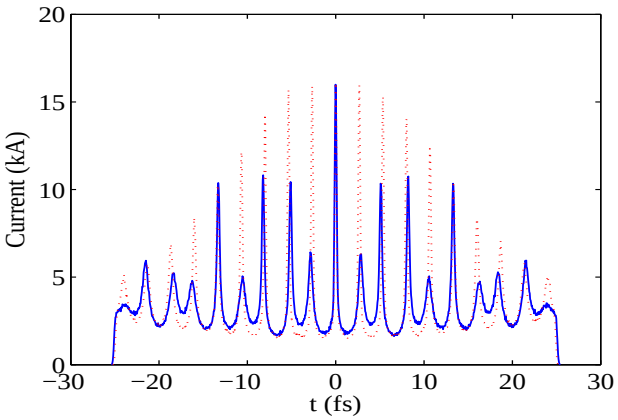

FIG. 3: (color) Current profile after a bunching chicane. Solid blue curve is from the interaction with two optimized lasers, while red dotted curve is from Laser-1 only.

where $r = \sqrt{x^2 + y^2}$, $Z_0 = 377\ \Omega$, $I'(s) = dI/ds$ is the derivative of the electron current profile with respect to the longitudinal bunch coordinate s, σ_z is the rms bunch length, and r_b is the beam radius of a uniform transverse distribution. Here we take $\bar{\gamma}_z \sim 10000$, $r_b \approx 2\sigma_x \sim 60\ \mu$m, and central spike $\sigma_z \sim 40$ nm. With these parameters, E_z depends very weakly on the transverse position of the electrons within the beam. Hence we drop the r-dependent term in computing the LSC field.

Figure 4 shows the accumulated energy modulation due to the LSC effect at a distance of 50 m in the FEL undulator. For the central current spike, LSC produces a strong energy chirp with a peak-to-peak energy variation of about 30 MeV, much larger than the FEL bandwidth. Such a large energy spread can degrade the FEL interaction as illustrated in *GENESIS* 1.3 [17] simulations that include LSC. A typical radiation profile at 50 m is shown in Fig. 5, where the normal undulator parameters of LCLS were used, i.e., $\lambda_u = 3$ cm, $K = 3.5$ and average beta function of 18 m in the undulator. We can see that although the peak current at the bunch center is over 17 kA, the radiation is still suppressed due to a large energy chirp created from the LSC force.

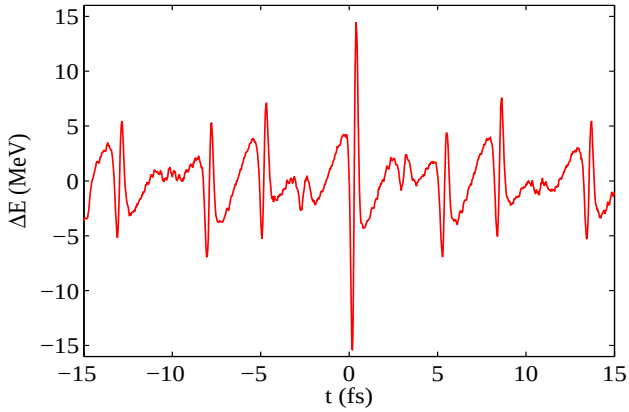

FIG. 4: (color) Electron bunch energy modulation from the LSC field after a distance of 50 m in the LCLS undulator. The bunch head is to the right, as in the following figures.

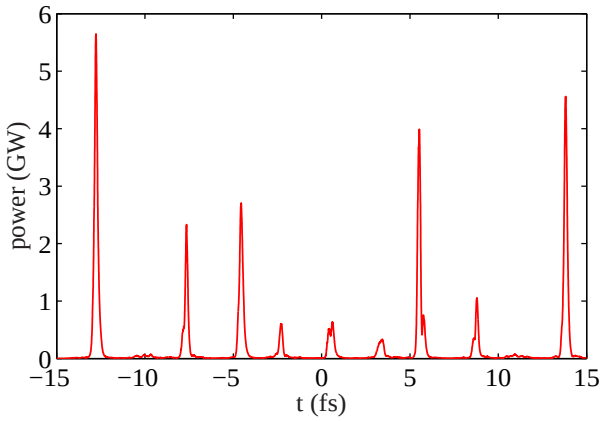

FIG. 5: (color) A typical example of the radiation profile at an undulator distance of 50 m without any undulator tapering. Large energy spread induced from LSC in the bunch center degrades the FEL interaction.

IV. SINGLE ATTOSECOND SPIKE SELECTION USING TAPERED UNDULATORS

It has been pointed out in Ref. [7] that a tapered undulator can compensate for the FEL gain degradation induced by a linearly chirped electron beam entering the undulator. In the case of ESASE with high-current spikes, LSC in the FEL undulator produces an almost linear energy chirp within these spikes that also grows in proportion to the undulator distance. As the radiation wave slips to the front of the current spike, the energy of the electrons in the

front part of the current spike increases due to LSC and upsets the resonant condition. This is the main reason for the suppression of the FEL gain as shown in Fig. 5. By tapering the undulator parameter, K, we can compensate for the energy change to a large extent, and preserve the resonant condition for the interacting part of the electrons. However, because the strength of the LSC fields depends on the derivative of the current, the proper taper strength is stronger for the central peak than for the side peaks. In our scheme, the energy modulation for the central peak is about a factor of 2 larger than for the side ones (see Fig. 4). By choosing the taper to match the strongest chirp of the central peak, we can preserve the resonant condition in this region, while simultaneously suppressing the FEL process elsewhere in the bunch. In addition, the larger current at the central peak produces a higher FEL gain than at the side peaks. Hence the combination of the enhanced current and undulator taper can provide a good contrast ratio between the central and side x-ray spikes.

We use *GENESIS* to find the undulator taper that optimizes the contrast ratio between the central and side spikes in the radiation pulse. Tapers used to compensate for energy loss from radiation require K to decrease along the undulator; in contrast, here we require an undulator taper with increasing K (defined as a negative taper in [7]) to offset the energy chirp from LSC in the central current peak of the bunch. Fig. 6 shows the x-ray power profile using a negative taper of 1% from 15 m to 70 m. The result in this figure is averaged over 10 shot noise realizations because of large statistical fluctuations on each spike. A good contrast ratio of $\sim$20 is obtained between the central and side spikes. The averaged peak power is 2.3 ± 1.5 GW at 50 m and the FWHM of the central spike is about 110 attoseconds. The taper used here is optimized to get the best contrast ratio between the central and side spikes, which is stronger than the taper giving maximum radiation power for the central spike. This suppresses the power of the central spike by $\sim$20%. Compared to the more uniform electron bunch of the normal LCLS configuration, the two-color ESASE scheme discussed here shows strong FEL slippage effects in the narrow current spike region. As a result, the x-ray spike duration obtained here is shorter than the typical LCLS SASE spike of 300 attoseconds, but the saturated FEL power is also reduced.

As the the electron energy is strongly chirped due to LSC within the central spike, we expect the attosecond ESASE spike to be frequency-chirped. This radiation chirp was discussed in [7, 18] where a fixed energy chirp formed before electrons entered the undulator.

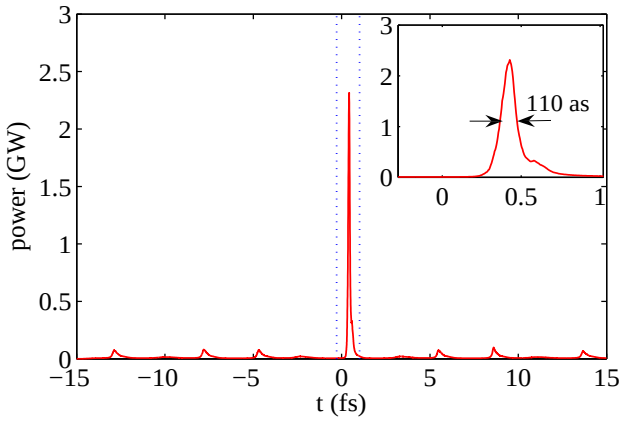

FIG. 6: (color) X-ray power profile (averaged over 10 shot noise realizations) at an undulator length of 50 m with an optimized undulator tapering of 1% from 15 m to 50 m. The inset zooms to the central spike in the dotted blue region.

In our case, the electron energy chirp changes while electrons move through the undulator, complicating the radiation chirp. From *GENESIS* simulations, we analyzed this radiation chirp using the on-axis far field radiation. The Wigner function $W(\omega, t)$ can be constructed from the radiation field to get a time-frequency "phase space" of the radiation:

$$W(\omega, t) = \int d\tau E(t - \frac{\tau}{2}) E^*(t + \frac{\tau}{2}) e^{i\omega\tau}. \tag{2}$$

An example calculated from Eq. (2) is shown in Fig. 7. The chirp analyzed from 10 shot noise realizations is $(3.4 \pm 0.7) \times 10^{-2}$Å$/fs$. The frequency chirp over the attosecond pulse is larger than the intrinsic FEL bandwidth and is visible from Fig. 7.

V. COHERENT CONTROL OF THE X-RAY RADIATION PULSE

The second laser wavelength is optimized to be 1.314 μm to obtain a single spike x-ray pulse (single mode), as shown in Fig. 6. The laser and undulator taper are optimized to suppress the side spikes in the radiation pulse. From the laser technique, this second laser can be tunable between 1.3 to 2 μm [12]. By tuning the wavelength of Laser-2 we can adjust the contrast ratio between the central and side spikes in the current profile, hence the intensity of the side spikes in the x-ray radiation pulse can be coherently controlled.

The taper of the main undulator is fixed at the optimized value to generate a single attosecond pulse, i.e., a negative taper of 1% from 15 m to 70 m in our studies. Then

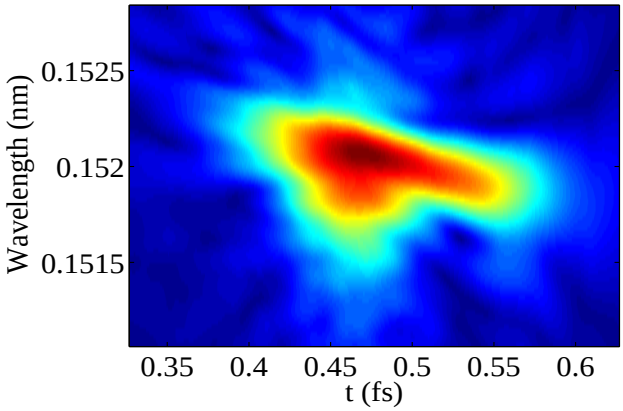

FIG. 7: (color) False color image of the Wigner transform of the on-axis far field radiation at an undulator length of 50 m.

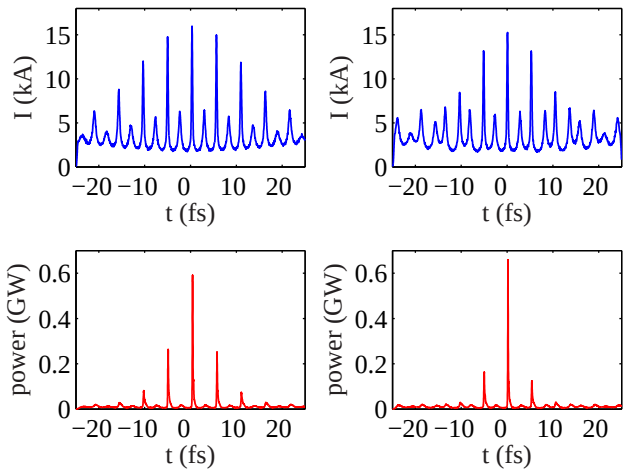

FIG. 8: (color) Current profiles (top) and radiation pulses (bottom) versus detuning of the second laser wavelength. Left: Laser-2 wavelength of 1.6 μm; Right: Laser-2 wavelength of 1.45 μm.

the Laser-2 wavelength is tuned from 1.6 μm down to 1.3 μm to control the current profile of the electron bunch. We performed simulations at Laser-2 wavelength of 1.6 μm and 1.45 μm. Fig. 8 shows the current profiles and corresponding radiation pulses at these two wavelengths of Laser-2. At a wavelength of 1.6 μm for Laser-2, all but four of the side peaks are suppressed. Suppression of side spikes continues when tuning Laser-2 down to 1.45 μm, then reaching the single spike mode at the wavelength of 1.314 μm as described in Fig. 6 in the previous section.

VI. SUMMARY AND DISCUSSIONS

In this paper, we propose an attosecond x-ray FEL scheme using relatively long commercially available infrared laser pulses. This scheme builds on the two-color ESASE proposal [6] that uses extremely short laser pulses shared by other attosecond schemes. Our scheme makes use of a tunable second laser wavelength which can coherently control the number of spikes and the pulse duration of the output x-rays. By properly taking into account the LSC field in the FEL undulator, we show that a tapered undulator can further suppress the side peaks in the radiation pulse and enable the selection of a single ~ 110 attoseconds x-ray spike. The peak power of the attosecond spike at the FEL saturation is about 2.3 GW, a factor of 20 larger than the nearest side peaks and a factor of 200 larger than the radiation power generated from an unmodulated electron beam.

Controlling the phase shift between the two lasers is a critical issue in the two-color ESASE scheme. Figure 9 shows an example of the radiation profiles assuming a phase shift of $\pm 0.1 fs$ between the two lasers, with five runs for each phase shift using different shot noise realizations. Compared with Fig. 6, the central spike locations shift about $\pm 0.1 fs$, and the contrast ratio between the central and side spikes is also reduced from $\sim$20 to $\sim$10. We note that this phase stability is intrinsically achieved in the optical parametric amplifier set-up for the laser system in our considerations. Mechanical instabilities are usually circumvented using a stable table-top laser set-up combined with active adaptive optics.

VII. ACKNOWLEDGEMENTS

We would like to thank A. Zholents and W. White for useful discussions. This Work was partially supported by the U.S. DOE contract DE-AC02-76SF00515.

---

[1] E.L. Saldin, E.A. Schneidmiller, and M.V. Yurkov, Opt. Commun. **212**, 377 (2002).

[2] A. A. Zholents and W. M. Fwaley, Phys. Rev. Lett. **92**, 224801 (2004).

[3] E.L. Saldin, E.A. Schneidmiller, and M.V. Yurkov, Opt. Commun. **237**,153 (2004).

[4] E.L. Saldin, E.A. Schneidmiller, and M.V. Yurkov, Opt. Commun. **239**,161 (2004).

[5] P. Emma, Z. Huang, M. Borland, in Proceedings of FEL2004 (Trieste, Italy, 2004).

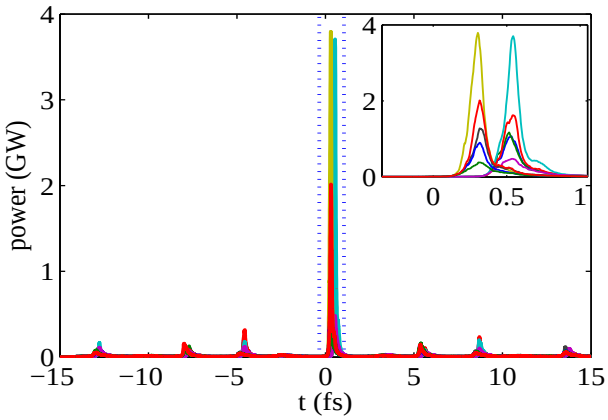

FIG. 9: (color) Radiation profiles with a phase shift of 0.1fs and -0.1fs between the two lasers, five runs for each phase shift using different shot noise realizations. The inset zooms to the central spikes in the dotted blue region.

[6] A. A. Zholents and G. Penn, Phys. Rev. ST-AB **8**, 050704 (2005).

[7] E.L. Saldin, E.A. Schneidmiller, and M.V. Yurkov, Phys. Rev. ST-AB **9**, 050702 (2006).

[8] A. A. Zholents and M S Zolotorev, New J. Phys. **10**, 025005 (2008).

[9] A. A. Zholents, Phys. Rev. ST-AB **8**, 040701 (2005)

[10] G. Geloni *et al.*, Nucl. Instrum. Methods A **583**, 228 (2007)

[11] H. Merdji *et al.*, Opt. Lett. **32** 3134 (2007).

[12] C.Vozzi, *et al*, Opt Express, **14**, 10109 (2006);C. Vozzi *et al.*, Opt. Lett. **32** 2957 (2007).

[13] LCLS Conceptual Design Report, SLAC-R-593 (2002).

[14] TESLA Technical Design Report, TESLA FEL 2002-09 (2002).

[15] SPring-8 Compact SASE Source Conceptual Design Report, http://www-xfel.spring8.or.jp (2005).

[16] A. W. Chao, *Physics of collective beam instabilities in high energy accelerators* (John Wiley & Sons, 1993).

[17] S. Reiche, Nucl. Instrum. Methods **A** 429, 243 (1999).

[18] W.M. Fawley, Nucl. Instrum. Methods **A** 593, 111 (2008).